Geophysical Research Letters

RESEARCH LETTER
10.1029/2019GL085653

Quantifying Asynchronicity of Precipitation and Potential Evapotranspiration in Mediterranean Climates

Xue Feng[1], Sally E. Thompson[2], Ross Woods[3], and Amilcare Porporato[4]

[1]Department of Civil, Environmental and Geo-Engineering & Saint Anthony Falls Laboratory, University of Minnesota, Minneapolis, MN, USA, [2]Department of Civil, Environmental and Mining Engineering, University of Western Australia, Perth, Western Australia, Australia, [3]Department of Civil Engineering, University of Bristol, Bristol, UK, [4]Department of Civil and Environmental Engineering and Princeton Environmental Institute, Princeton University, Princeton, NJ, USA

Abstract Recent climate change has contributed to shifts in the seasonal interplay between precipitation and potential evapotranspiration, which have in turn increased droughts and reduced freshwater availability in Mediterranean climate regions. To overcome limitations in existing indices for comparing these seasonal hydroclimatic drivers at the global scale, we introduce an information theory-based, nonparametric asynchronicity index that captures both the temporal alignment and relative magnitudes of precipitation and potential evapotranspiration. We use this asynchronicity index to first identify Mediterranean climates around the world. We then apply the asynchronicity index over two Mediterranean climate regions and show that their boundaries have shifted between 1960 and 2018, resulting in a regional expansion in the U.S. Pacific Northwest and a contraction in southwestern Australia. These results highlight the need for globally consistent measures of seasonal climatic water supply and demand for diagnosing potential changes in water resources and ecosystem responses within Mediterranean climate regions.

Plain Language Summary Climate change is likely to change the boundaries of what are typically considered Mediterranean climate regions, which have dry summers and mild, wet winters. To analyze how these regions' water availability may be influenced by climate change, we introduce a metric for quantifying the mismatch in the timing and amount of precipitation relative to atmospheric water demand. This new metric is able to identify the boundaries of Mediterranean climate regions more effectively than other existing indices and can be used to analyze how these boundaries shift over time.

Key Points:
- A new metric is proposed to measure the seasonal mismatch between atmospheric water supply (precipitation) and demand (potential evapotranspiration, PET)
- Compared to existing metrics, the proposed metric can more accurately distinguish between climates with synchronized versus desynchronized seasonal signals of precipitation and PET
- Mediterranean climates are characterized by high climate asynchronicity, and their geographical extents have expanded in the U.S. Pacific Northwest and contracted in Western Australia since the turn of the century

Supporting Information:
- Supporting Information S1

Correspondence to:
X. Feng,
feng@umn.edu

Citation:
Feng, X., Thompson, S. E., Woods, R., & Porporato, A. (2019). Quantifying asynchronicity of precipitation and potential evapotranspiration in Mediterranean climates. *Geophysical Research Letters*, *46*. https://doi.org/10.1029/2019GL085653

Received 3 OCT 2019
Accepted 28 NOV 2019
Accepted article online 9 DEC 2019

1. Introduction

Bioclimatic classifications have been used for centuries (Varenius, 1650; von Humboldt, 1820) to help identify climates with similar characteristics (Oliver, 1991), associate climates with key environmental and biodiversity indicators (Metzger et al., 2013), and to transfer known landscape responses within one climate to another in which less is known (Razavi & Coulibaly, 2013). For example, multiple bioclimatic classifications have proposed metrics of climate aridity (Budyko & Miller, 1974) to identify regions that might suffer from climatic water deficits. These aridity (or dryness) indices are then adopted within hydrological sciences to predict the proportion of precipitation that typically generates streamflow (Berghuijs et al., 2014; D. Wang & Hejazi, 2011); within ecological sciences to predict biodiversity, ecosystem health, and biogeochemical cycling (Maestre et al., 2015; C. Wang et al., 2014); and within agricultural sciences to predict crop yields and to design irrigation schemes (Bannayan et al., 2010; Paltineanu et al., 2007; Vico & Porporato, 2015). Despite the wide use of bioclimatic classifications for contextualizing a range of natural phenomena, the boundaries of bioclimatic regions as they are currently defined—and the ecosystem and catchment responses that are associated with them—will likely change in a warming world (Staten et al., 2018; Thomas & Nigam, 2018). In particular, Mediterranean-climate regions—places whose climates are characterized by dry summers and mild, wet winters, generally located along western continental margins (see, e.g., Barry & Chorley, 2009)—are thought to be especially vulnerable to water deficit resulting from climate change (Diffenbaugh & Giorgi, 2012; Klausmeyer & Shaw, 2009; Underwood et al., 2009).

In Mediterranean climates, changes to freshwater availability result not only from direct reduction in total annual precipitation volumes or increases in evaporative demand due to rising temperatures (Diffenbaugh et al., 2015) but also from changes in how precipitation and potential evapotranspiration (PET) interact at

seasonal time scales. For example, in Mediterranean climates, plant water use—which makes up a large part of the water budget—are energy-limited during the winter and water-limited during the summer (Ryu et al., 2008). As the climate warms, increase in plant water use in Mediterranean climates due to higher-energy availability in spring can be offset by decreases due to soil limitation in summer (Pangle et al., 2014; Tague & Peng, 2013), a phenomena consistent with global trends (Angert et al., 2005; Buermann et al., 2018; Wolf et al., 2016). This temporal alignment of seasonal water and energy availability (or its change) also influences partitioning of subsurface water resources between groundwater recharge, transpiration, and streamflow (Dralle et al., 2018; Hahm et al., 2019). Additionally, in Mediterranean climates that are snow-dominated, warming reduces the fraction of precipitation that falls as snow and promotes earlier snowmelt (which is slower and less likely to saturate soils; Musselman et al., 2017): all changes that tend to increase evapotranspiration at the expense of streamflow (Barnhart et al., 2016). However, earlier snowmelt also tends to concentrate snowmelt during colder periods when transpiration rates are low, an effect that may actually reduce the annual proportion of transpiration relative to streamflow (Jeton et al., 1996; Winchell et al., 2016). Thus, the outcome of changing hydroclimatic processes on water resources in these regions depends on the interactions of snowmelt, soil water availability, and vegetation water use, which in turn result from shifts in the relative magnitude and timing of the seasonal water and energy inputs.

While the importance of considering trade-offs between water and energy availability on annual scales has long been known and forms a central organizing framework in hydroclimatology (Budyko & Miller, 1974), globally applicable measures of how well aligned climatic water and energy supply are—that is, their *synchronicity*—on within-year, seasonal time scales are conspicuously lacking. Yet it is exactly this synchronicity—or rather its absence, or asynchronicity—which is the defining characteristic of Mediterranean climates. Therefore, to monitor ongoing alterations to existing boundaries around vulnerable Mediterranean climates, and to advance understanding of changing ecological and hydrological responses within these climate regions, a globally applicable measure of hydroclimatic synchronicity is needed.

Many existing metrics of hydroclimatic seasonality and synchronicity are limited in their ability to fully capture the seasonal dynamics of precipitation and PET. For example, synchronicity in precipitation relative to PET is often quantified by the phase lag between their climatologies (Berghuijs & Woods, 2016; Gentine et al., 2012; Potter et al., 2005). This measure describes the relative timing of peaks in precipitation and PET signals but does not capture the intensity of the seasonal variation in each. In omitting this, phase-lag metrics exclude information about the degree of variations in precipitation and PET between wet/dry or summer/winter periods—features that distinguish many "out-of-phase" (or asynchronous) Mediterranean regions (Viola et al., 2008) from other seasonally dry climates (e.g., tropical dry and monsoon climates) with more uniformly distributed PET, which are dominated by a different set of climatically mediated plant water use strategies (Vico et al., 2014) and soil water partitioning (Feng et al., 2012). In addition, most metrics (e.g., Milly, 1994) assume that both precipitation and PET must vary sinusoidally across the year, thus cannot be immediately applied to many parts of the world that do not have smooth transitions between seasons without additional assumptions.

Here, we introduce a new metric of climate asynchronicity based on information theory. This metric captures the entire within-year distributions of precipitation and PET, in terms of both their relative magnitudes and phase differences. It is nonparametric and does not assume sinusoidality, unimodality, or a constant period for the annual climatic signals. We apply this asynchronicity index across the world using a global climatology data set CRU TS v.4.03 (Harris et al., 2014) and demonstrate its superior ability, compared to prevailing metrics of seasonality, to distinguish between climates whose precipitation and PET climatologies are asynchronous (i.e., in Mediterranean climates) versus synchronous (e.g., in other seasonal climates). Additionally, we use this metric to illustrate changing patterns of climate asynchronicity, finding that since the turn of the century, Mediterranean climates have grown out of semiarid climates in the U.S. Pacific Northwest and shrunk as they transform into semiarid climates in Western Australia.

2. Methods

2.1. Asynchronicity Index Defined

We adopt an information theory-based metric—the Jensen-Shannon distance (Endres & Schindelin, 2003)—to quantify the degree of asynchronicity between two generic random variables, P and Q, whose

domains are nonnegative. Assuming that P and Q are randomly distributed at monthly time scales, we take their long-term mean monthly values $\overline{r}_m$ and $\overline{k}_m$ (where the overbar indicates the long-term mean and the index $m \in [1,12]$ indicates the month of the calendar year) and calculate their discrete probability mass functions (pmfs, where the probability of P is indicated by p and the probability of Q by q), denoted by $\overline{p}_m = \overline{r}_m / \sum_{m=1}^{12} \overline{r}_m$ and $\overline{q}_m = \overline{k}_m / \sum_{m=1}^{12} \overline{k}_m$.

The Jensen-Shannon distance measures how *dissimilar* any two random variables are; in this case, it measures the total divergence of the two probability distributions from their average, that is,

$$JS = \sqrt{\frac{1}{2}\overline{D}_{P|N} + \frac{1}{2}\overline{D}_{Q|N}}, \tag{1}$$

where $\overline{D}_{P|N}$ and $\overline{D}_{Q|N}$ are the relative entropies (Kullback & Leibler, 1951) of P and Q with respect to their average $N = \frac{1}{2}(P+Q)$. The relative entropies are computed as $\overline{D}_{P|N} = \sum_{m=1}^{12} \overline{p}_m \log_2\left(\frac{\overline{p}_m}{n_m}\right)$ and $\overline{D}_{Q|N} = \sum_{m=1}^{12} \overline{q}_m \log_2\left(\frac{\overline{q}_m}{n_m}\right)$, with $n_m = \frac{1}{2}(\overline{p}_m + \overline{q}_m)$.

The asynchronicity index *ASI* is then defined as square root of the difference between the observed Jensen-Shannon distance (JS_{obs},as calculated from equation (1)) and the minimized Jensen-Shannon distance that can be achieved for the seasonal profiles of P and Q at that location:

$$ASI = \sqrt{JS_{obs} - JS_{min}} \tag{2}$$

The minimum Jensen-Shannon distance JS_{min} can be thought of as the Jensen-Shannon difference that emerges from the temporal configuration of P and Q that results in the *most* overlap between the random variables. To compute JS_{min}, the observed distributions of one of the random variables, Q, is shifted by an increment of w months, where $w \in [1,12]$. This results in a new pmf $\overline{q}_m^w = \overline{q}_{m-w}$, and consequently in a new average N^w, associated (new) values of $\overline{D}_{P|N}^w$ and $\overline{D}_{Q|N}^w$, and a new Jensen-Shannon distance, JS_w. JS_{min} is finally selected by finding the value of w minimizing JS_w, that is,

$$JS_{min} = \min(JS_w), w \in [1, 12] \tag{3}$$

The two-step process of finding the divergences of P and Q and then subtracting JS_{min} from JS_{obs} captures the effects of two sources of desynchronization between P and Q: (i) One in which their pmfs differ in relative magnitudes and (ii) one in which one random variable is shifted relative to the other. Theoretically, the values of the asynchronicity index are bounded on the lower side by $ASI = 0$, when P and Q have the same pmf, and on the upper side by $ASI = 1$, when the domains of P and Q fail to overlap during any months of the year but can be shifted to achieve complete overlap.

When the asynchronicity index (*ASI*, equation (2)) is applied to the monthly pmfs of precipitation and PET, it encapsulates information about both (i) the relative magnitudes of the normalized climatic forcings and (ii) the temporal shift it would take for maximum synchronization to occur. These attributes are illustrated using synthetically generated monthly sinusoidal distributions of precipitation and PET in Figure 1 (see supporting information for more details on the synthetic time series), where *ASI* monotonically increases with increasing relative magnitudes (RM, given by the ratio of the amplitudes of the sinusoidal functions) and phase differences (ϕ) between precipitation and PET distributions. As shown in this figure, a large *ASI* value at a location arises when the precipitation and PET pmfs are mismatched in timing and magnitude (e.g., where RM = 1 and ϕ = 6 months), situations which might correspond to Mediterranean type climates. Lower values of *ASI* arise where the pmfs are in phase (e.g., the $\phi = 0$ case), which could correspond to climates with summer precipitation maxima, and if one of the climate attributes lacks seasonal variation (e.g., the RM = 0 case), which could correspond to climates having a seasonally concentrated wet season but relatively uniform PET year round, including some tropical and tropically dry climates. Because the *ASI* is calculated from pmfs (i.e., the absolute values of its constituent random variables are normalized), it is invariant when P and Q are scaled by a common factor. However, the *ASI is* sensitive to transformations

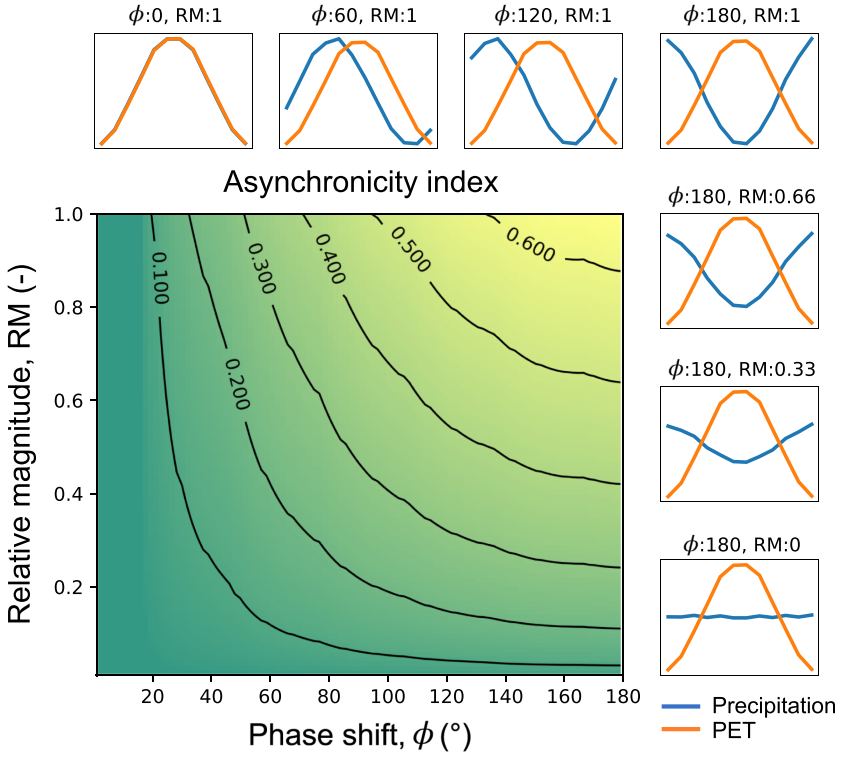

Figure 1. Variation of the Asynchronicity Index between two synthetic, sinusoidal precipitation, and potential evapotranspiration (PET) probability mass functions (pmfs) at the monthly scale. The subplots illustrate various combinations of seasonal distributions of precipitation (in blue) and PET (in orange), with pmfs plotted across months. RM is the relative magnitude of the pmfs, given by the ratio of their amplitudes; ϕ measures their phase shifts.

that affect the relative scales of variations. For example, if the datum of the variables were shifted, or if the variables were obtained through different units (e.g., precipitation in inches instead of millimeters), then the same amount of absolute variation would result in different relative variations that register within the *ASI*. In such cases, care should be taken to ensure consistency across different stations and across different transformations.

2.2. Using Asynchronicity Index to Delineate Mediterranean Climates

We mapped asynchronicity index (*ASI*) worldwide using the CRU TS v.4.03 gridded climate data set, which includes long-term reanalysis of monthly precipitation and PET time series from 1901 to 2018 at 0.5° resolution (Harris et al., 2014). We derived the long-term climatology, and the seasonal distributions of precipitation and PET, $\overline{p}_m$ and $\overline{q}_m$ within each grid cell using this data set and then computed ASI with equations (1) and (2). The resulting global distribution of *ASI* is shown in supporting information Figure S1.

To designate a location as climatically "synchronized" or "desynchronized" according to the *ASI*, we relied on known distributions of climate types around the world. In particular, we used the "Cs-" ("Mediterranean climate") groups within the Köppen-Geiger classifications (Kottek et al., 2006) to delineate areas known to have "desynchronized" climates. To relate "desynchronized" climates to values of *ASI* that might define such climates, we generated empirical frequency distributions of *ASI* for each seasonal climate type: "Cs-" groups within the Köppen-Geiger classifications are designated as "Mediterranean," "BW-" groups are "desert," "BS-" groups are "semiarid," "Am" is "monsoon," "Aw" is "tropical dry," "Af" is "tropical," and "Cfa" is "humid subtropical." Then, using fitted empirical cumulative distribution functions (ecdf), we identified the *ASI* value that maximized the difference between the ecdf of Mediterranean regions and the ecdf of climatically adjacent, semiarid regions (see supporting information for more details). This value, found to be $ASI = 0.36$, represents the threshold that includes the largest proportion of Mediterranean climates while excluding the largest proportion of semiarid climates worldwide.

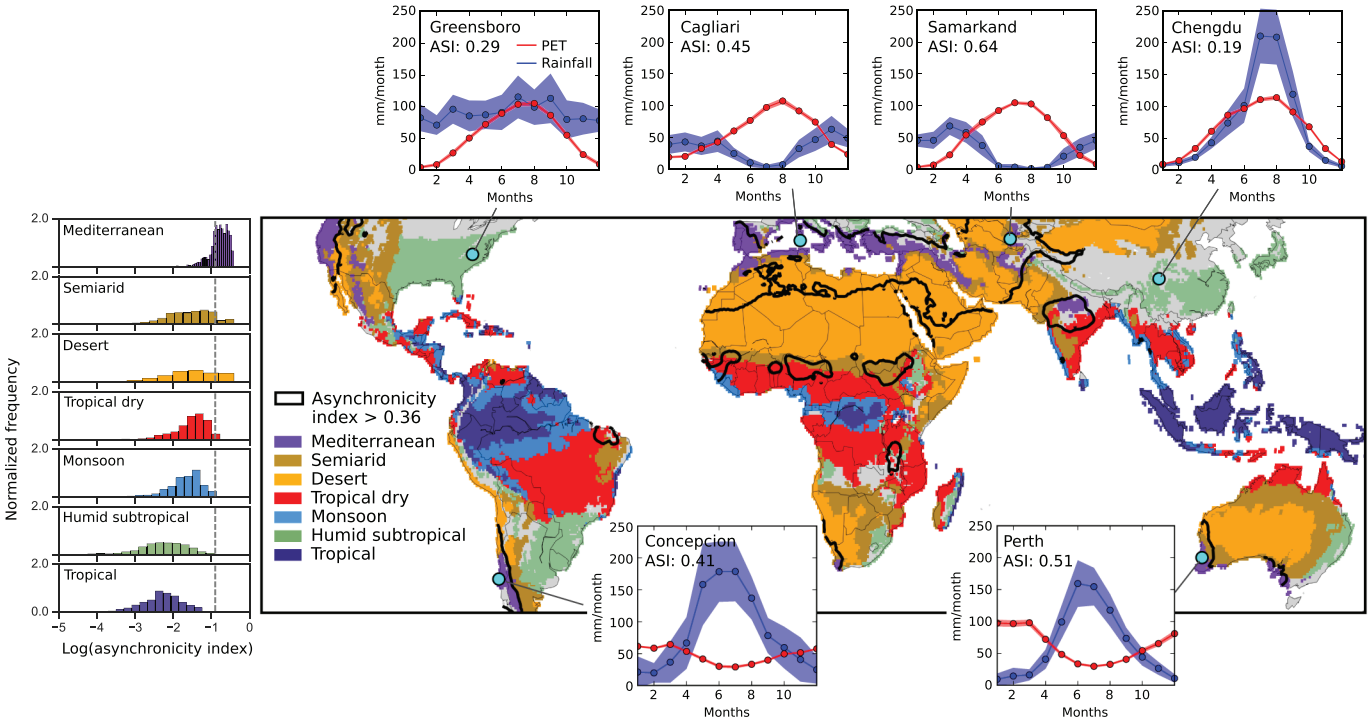

Figure 2. Global distributions of seasonal Köppen-Geiger climate types (Kottek et al., 2006) from 45°S to 45°N, along with outline of the areas where asynchronicity index is above a critical threshold of $ASI = 0.36$. The frequency diagrams show the frequency distribution of the asynchronicity index in each climate regions, and the dashed line represents the critical threshold (in log scale, with log $(ASI = 0.36) = -1.0$).

2.3. Comparisons With Other Indices of Climate Seasonality

To evaluate the ability of the asynchronicity index to delineate the geographical boundaries of Mediterranean climates relative to those of other seasonal climates, we adopt a common diagnostic metric of a binary classifier: The area under curve (AUC) of the receiver operating characteristics (ROC) curve (Fawcett, 2006; Hanley & Mcneil, 1982). The ROC curve is produced by plotting the true positive rate of classifications made using a metric against the false positive rate, across a range of threshold values defining the classifier. In this case, the true positive rate is given by the proportion of Mediterranean climates ("Cs-"groups within the Köppen-Geiger classification) worldwide identified by a given metric value, and the false positive rate is given by the proportion of other seasonally dry climates ("BS-," "Am," and "Af" groups within the Köppen-Geiger classification) identified by the same metric value. By integrating the true positive rate across the entire range of false positive rates, the AUC-ROC tells us about the ability of a metric to distinguish between Mediterranean versus seasonal climates: an AUC of one indicates complete separability, while an AUC of 0.5 indicates that the metric is completely uninformative (i.e., equivalent to a coin toss).

We calculated the AUC-ROC for seven exiting metrics of climate seasonality to compare their ability to distinguish Mediterranean climates within the Köppen-Geiger classification from other seasonally dry climates: (1) The current proposed asynchronicity index (*ASI*), (2) the centroid difference (in months) between the seasonal precipitation and PET pmfs (i.e., *dCentroid*), and a series of seasonality indices proposed by (3) Walsh and Lawler (1981) (i.e., *WalshS*), (4) Milly (1994) (i.e., *MillyS*), (5) Woods (2009) (i.e., *dP**), (6) Feng et al. (2013) (i.e., *SI*), and (7) Knoben et al. (2018) (i.e., *Imr*). Brief explanations of these metrics and their abbreviations are summarized in Table S1.

2.4. Regional Shifts in Mediterranean Regions

Based on an initial global analysis of changes in the location of the $ASI = 0.36$ threshold over time in the CRU TS v. 4.03 data set, we identified regional shifts in Mediterranean regions worldwide, including

conspicuous changes in the U.S. west coast (California and Pacific Northwest regions) and the Australian southwest coast (including near Perth and Adelaide). We explored how *ASI* in these regions varied across different time periods (1960–1979, 1980–1999, and 2000–2018) and mapped the resulting contours of *ASI* = 0.36 over current Köppen-Geiger classifications (Kottek et al., 2006) to see how the boundaries of these Mediterranean climates shifted over times.

3. Results and Discussions

3.1. Asynchronicity Index Captures the Global Distribution of Mediterranean Climates

Comparing the *ASI* in different climate regions in the Köppen-Geiger system (Kottek et al., 2006) shows that it is a useful indicator of Mediterranean climates worldwide (Figure 1). From the frequency diagrams in Figure 1, it can be seen that a majority of Mediterranean regions exhibit *ASI* values that are substantially larger than those found in most other tropical and midlatitude climates. Furthermore, the areas where asynchronicity index exceeds the critical threshold of $ASI = 0.36$ (the climatically "desynchronized" regions) capture well the geographical extent of Mediterranean climates around the world, especially in California, Chile, tip of South Africa, the Indian subcontinent, and Australia.

In the Mediterranean basin in Europe and across much of Eurasia, high *ASI* values enclosed regions that are defined as semiarid and desert by the Köppen-Geiger system. This is likely because the Köppen-Geiger classification relies on minimum and maximum rainfall thresholds that are not factored into the asynchronicity index. Climatologically, semiarid and desert areas, despite experiencing low annual rainfall, can exhibit similar offsets in the seasonal patterns of precipitation and PET that are typical of Mediterranean climates. Semiarid and desert climates are also often found adjacent to Mediterranean climates and share related water scarcity and land management issues stemming from alternating seasonal cycles of water excess and scarcity. Together, these regions contain high levels of biodiversity (Cowling et al., 1996; Médail & Quezél, 1999) and generate more streamflow compared to other regions at comparable dryness (Farmer et al., 2003; Feng et al., 2015; Trancoso et al., 2017), but their water resources are increasingly challenged by climate change (Diffenbaugh et al., 2015; Giorgi, 2006), agricultural conversion, and irrigation use (Zhang & Oweis, 1999), with Mediterranean regions often considered to be at risk of aridification though declines in precipitation (Seager et al., 2014). By classifying these climates based on hydroclimatically relevant measures of seasonality, the asynchronicity index highlights their functional similarities and collective vulnerability.

The only major region with Mediterranean climate excluded by the asynchronicity index is in central Mexico, a region that has been shown to fulfill the Köppen-Geiger classification for both Mediterranean and humid subtropical climates and, which on further inspection of surrounding station data, was reclassified into the humid subtropical climate type by an updated study (Peel et al., 2007).

3.2. Asynchronicity Index Outperforms Other Indices for Finding Mediterranean Climates

Relative to other common metrics of climate seasonality tested, the asynchronicity index was best able to separate Mediterranean climates from other seasonally dry climates. The metrics' performances were evaluated using AUC of ROC, which is calculated independently of metric-specific thresholds. Nevertheless, we can still examine the maximum extent of separability that can be achieved by setting a specific metric value. At a threshold of $ASI = 0.36$, the proportion of Mediterranean climates with $ASI > 0.36$ is 91% (the true positive rate), while the proportion of other seasonal climates with $ASI > 0.36$ is 32% (the false positive rate). No other metric came close to achieving this level of separability (Figure 3) for Mediterranean versus other seasonal climates, because similar metric values also identified areas that were seasonal but synchronized, resulting in large overlaps in the pdf of metric values for Mediterranean versus other seasonal climates (Figure 3c) and thus large false positive rates at a given true positive rate (Figure 3e). This is perhaps unsurprising, since most of the other metrics were designed for the less specific task of identifying seasonal climates distinct from aseasonal climates.

Some limitations of the existing indices for capturing the full seasonal interactions between precipitation and PET include the following: *SI* and *WalshS* are applicable to only a single climate variable (they were applied to precipitation rather than PET seasonality in this case, since this is a distinguishing feature of seasonally dry climates). *MillyS* and *dP** are bivariate metrics that capture variations in both precipitation and

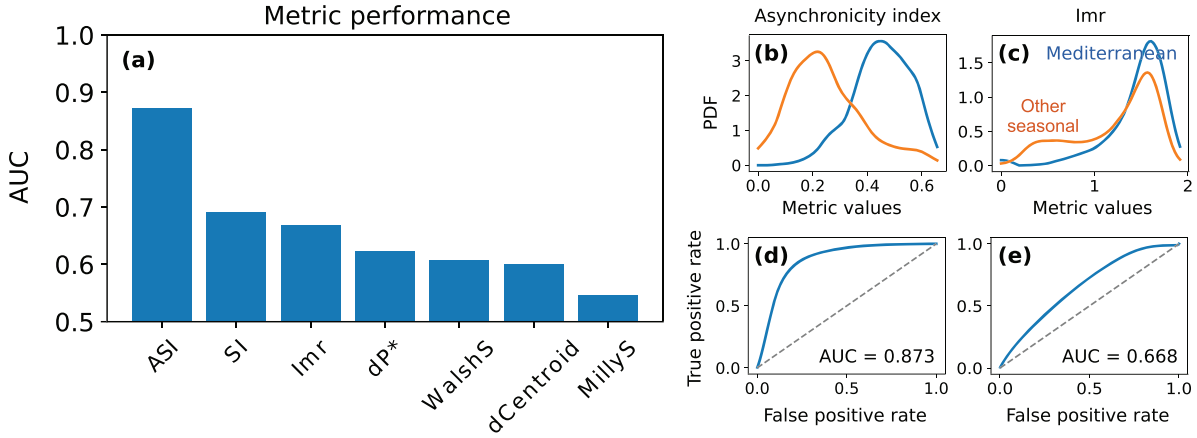

Figure 3. (a) Performance of Asynchronicity Index (*ASI*) relative to other metrics in distinguishing Mediterranean climates ("Cs-" groups in the Köppen-Geiger classification) from other seasonal climates (tropical wet/dry, monsoon, hot semiarid, or "BS-," "Am," and "Af" groups) using area under the curve (AUC) of the receiver operating characteristic curve. The *x* axis is truncated at 0.5 because it corresponds to the metric being completely uninformative. (b and c) The frequency of Mediterranean climates versus other seasonal climates that are identified by the *ASI* and Knoben's seasonality index (*Imr*) over the range of their values. (d and e) The true positive rate versus false positive rate for identifying Mediterranean climates against other seasonal climates associated with the *ASI* and *Imr*, plotted over the range of their values. These are the receiver operating characteristic curves from which AUC values are derived.

PET but require that they vary sinusoidally. Consequently, errors can result from approximating the seasonal distributions with sinusoidal functions. Of the two characteristics of P and PET that can contribute to their seasonal desynchronization, *dCentroid* considers only their timing difference, and *MillyS* considers only their relative magnitudes. Both *Imr* and *ASI* account for the relative magnitudes of precipitation and PET in each month, but only *ASI* does so by integrating those differences across the entire year.

3.3. Asynchronicity Index Illustrates Shifts in Boundaries of Mediterranean Climates

By applying the asynchronicity index to precipitation and PET time series to identify climatically "desynchronized" regions over time, we identified shifts in the geographical boundaries of what would typically be considered Mediterranean regions. These shifting boundaries are illustrated for the western U.S. and southwestern Australia in Figure 4 over three time periods: 1960–1979, 1980–1999, and 2000–2018.

In the western U.S., the boundaries of climatically desynchronized regions have steadily expanded from the west coast states (California, Oregon, and Washington) in the 1960s over more inland states like western Idaho and Nevada after the turn of the century. This shift now encompasses some areas that are currently classified as semiarid or desert in the Inland Pacific Northwest and is consistent with most global circulation models that project in this region a small but systemic increase in precipitation during the winter and spring and a slight decrease in summer (IPCC, 2014). This shift in climate has prompted considerations of adopting new winter crops within the dryland dropping system in the Inland Pacific Northwest (Stöckle et al., 2018) and new conservation strategies for Pacific Northwest prairies and oak savannas (Bachelet et al., 2011).

In southwestern Australia, the boundaries of climatically desynchronized regions have steadily contracted since the 1960s, with previously Mediterranean-like regions now replaced by desert and semiarid climates. These shifts may be occurring due to changes in the seasonality of one or both precipitation and PET. For example, in southwestern Australia, observed trends in winter rainfall declines (Timbal et al., 2006) may cause the interior areas to have less precipitation seasonality, while increasing temperature and dryness at the same time may have results in increasing synchronicity between precipitation and PET. These climatic trends are accompanied by concomitant declines in stream yields in the drinking water catchments (Bates et al., 2008; Petrone et al., 2010) and negative impacts on the highly biodiverse ecosystems in this region (Brouwers et al., 2013), including tree mortality events observed through satellite and aerial imaging (Evans et al., 2013; Evans & Lyons, 2013; Matusick et al., 2013). These climatic shifts challenge our conceptions of what constitutes a Mediterranean region, suggest that their boundaries can fluidly shift into and out

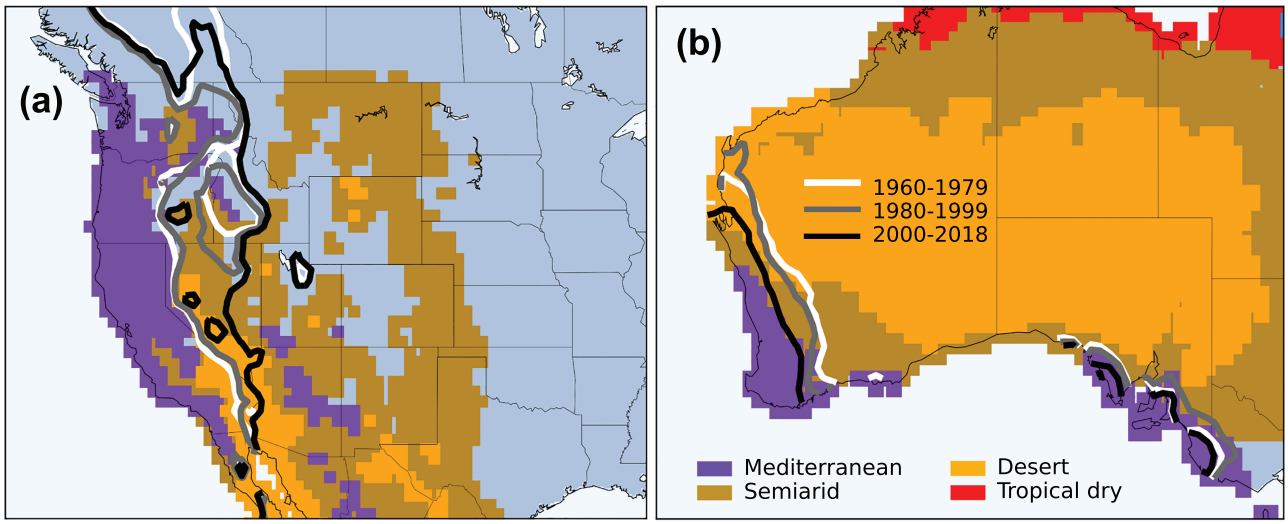

Figure 4. Changes in boundaries of asynchronicity index in (a) U.S. west coast and (b) southwestern Australia. Boundaries are calculated for the designated periods (1960–1979, 1980–1999, and 2000–2018) using the CRU TS v.4.03 data set. The underlying climates shown on the maps are based on the Köppen-Geiger classification from Kottek et al. (2006).

of their adjacent climate zones over a relatively short time period, and prompt us to adopt suitable tools for diagnosing these shifts and evaluating their impacts on the local landscapes.

4. Conclusions

We introduce here a new information theory-based asynchronicity index that is well suited to identify the extent of climatologically desynchronized (e.g., Mediterranean-like) regions globally. This approach differs from existing climate classification schemes, which are strongly informed by the biogeography of vegetation (e.g., Kottek et al., 2006) and rely heavily on the use of monthly minimum or maximum thresholds to describe biological presence or activity (Bazzaz, 1991; Kraft et al., 2014). This new metric selects seasonal climatic features that are known to influence the ecohydrology in seasonally dry regions—namely, the synchronicity in the precipitation and PET that arise from their relative magnitudes and timing—and is complementary to existing schemes (Budyko & Miller, 1974) for characterizing the seasonal interaction of precipitation and PET. We show that it outperforms exiting metrics of climate seasonality for characterizing Mediterranean regions and can be used to evaluate shifts in their geographical boundaries resulting from climate change. As Mediterranean regions have been identified as hot spots of both biodiversity (Cowling et al., 1996) and climate change (Giorgi, 2006) and face ongoing challenges associated with drought-induced water scarcity (Iglesias et al., 2007), a robust metric dedicated to identifying the climatic drivers of these challenges will be useful for evaluating future conservation and management priorities.

Acknowledgments
The authors would like to thank Salvatore Pascale, Athanasios Paschalis, and an anonymous reviewer for their constructive feedback on an earlier draft of the manuscript. Global data sets of the asynchronicity index and each of the seasonality index generated in the intercomparison (Table S1 and Figure 3), as well as the Python code used to generate the synthetic times series and the contour plot in Figure 1, are available at https://github.com/feng-ecohydro/seasonality-indices and on Hydroshare at Feng (2019).

References

Angert, A., Biraud, S., Bonfils, C., Henning, C. C., Buermann, W., Pinzon, J., et al. (2005). Drier summers cancel out the CO_2 uptake enhancement induced by warmer springs. *Proceedings of the National Academy of Sciences of the United States of America*, *102*(31), 10823–10827. https://doi.org/10.1073/pnas.0501647102

Bachelet, D., Johnson, B. R., Bridgham, S. D., Dunn, P. V., Anderson, H. E., & Rogers, B. M. (2011). Climate change impacts on Western Pacific Northwest Prairies and Savannas. *Northwest Science*, *85*(2), 411–429. https://doi.org/10.3955/046.085.0224

Bannayan, M., Sanjani, S., Alizadeh, A., Lotfabadi, S. S., & Mohamadian, A. (2010). Association between climate indices, aridity index, and rainfed crop yield in northeast of Iran. *Field Crops Research*, *118*(2), 105–114. https://doi.org/10.1016/j.fcr.2010.04.011

Barnhart, T. B., Molotch, N. P., Livneh, B., Harpold, A. A., Knowles, J. F., & Schneider, D. (2016). Snowmelt rate dictates streamflow. *Geophysical Research Letters*, *43*, 8006–8016. https://doi.org/10.1002/2016GL069690

Barry, R. G., & Chorley, R. J. (2009). *Atmosphere, weather and climate*. Milton, UK: Routledge.

Bates, B. C., Hope, P., Ryan, B., Smith, I., & Charles, S. (2008). Key findings from the Indian Ocean Climate Initiative and their impact on policy development in Australia. *Climatic Change*, *89*(3–4), 339–354. https://doi.org/10.1007/s10584-007-9390-9

Bazzaz, F. A. (1991). Habitat selection in Plants. *The American Naturalist*, *137*, S116–S130.

Berghuijs, W. R., & Woods, R. A. (2016). A simple framework to quantitatively describe monthly precipitation and temperature climatology. *International Journal of Climatology*, *36*(9), 3161–3174. https://doi.org/10.1002/joc.4544

Berghuijs, W. R., Woods, R. A., & Hrachowitz, M. (2014). A precipitation shift from snow towards rain leads to a decrease in streamflow. *Nature Climate Change*, *4*(7), 583–586. https://doi.org/10.1038/nclimate2246

Brouwers, N. C., Mercer, J., Lyons, T., Poot, P., Veneklaas, E., & Hardy, G. (2013). Climate and landscape drivers of tree decline in a Mediterranean ecoregion. *Ecology and Evolution*, *3*(1), 67–79. https://doi.org/10.1002/ece3.437

Budyko, M. I., & Miller, D. H. (1974). *Climate and life*. New York, NY: Academic Press.

Buermann, W., Forkel, M., O'Sullivan, M., Sitch, S., Friedlingstein, P., Haverd, V., et al. (2018). Widespread seasonal compensation effects of spring warming on northern plant productivity. *Nature*, *562*(7725), 110–114. https://doi.org/10.1038/s41586-018-0555-7

Cowling, R. M., Rundel, P. W., Lamont, B. B., Arroyo, M. K., & Arianoutsou, M. (1996). Plant diversity in Mediterranean-climate regions. *Trends in Ecology and Evolution*, *11*(9), 362–366. https://doi.org/10.1016/0169-5347(96)10044-6

Diffenbaugh, N. S., & Giorgi, F. (2012). Climate change hotspots in the CMIP5 global climate model ensemble. *Climatic Change*, *114*(3–4), 813–822. https://doi.org/10.1007/s10584-012-0570-x

Diffenbaugh, N. S., Swain, D. L., & Touma, D. (2015). Anthropogenic warming has increased drought risk in California. *Proceedings of the National Academy of Sciences*, *112*(13), 3931–3936. https://doi.org/10.1073/pnas.1422385112

Dralle, D. N., Hahm, W. J., Rempe, D. M., Karst, N. J., Thompson, S. E., & Dietrich, W. E. (2018). Quantification of the seasonal hillslope water storage that does not drive streamflow. *Hydrological Processes*, *32*(13), 1978–1992. https://doi.org/10.1002/hyp.11627

Endres, D. M., & Schindelin, J. E. (2003). A new metric for probability distributions. *IEEE Transactions on Information Theory*, *49*(7), 1858–1860.

Evans, B., & Lyons, T. (2013). Bioclimatic extremes drive forest mortality in southwest, Western Australia. *Climate*, *1*(2), 28–52. https://doi.org/10.3390/cli1020028

Evans, B., Stone, C., & Barber, P. (2013). Linking a decade of forest decline in the south-west of Western Australia to bioclimatic change. *Australian Forestry*, *76*(3–4), 164–172. https://doi.org/10.1080/00049158.2013.844055

Farmer, D., Sivapalan, M., & Jothityangkoon, C. (2003). Climate, soil, and vegetation controls upon the variability of water balance in temperate and semiarid landscapes: Downward approach to water balance analysis. *Water Resources Research*, *39*(2), 1035. https://doi.org/10.1029/2001WR000328

Fawcett, T. (2006). An introduction to ROC analysis. *Pattern Recognition Letters*, *27*(8), 861–874. https://doi.org/10.1016/j.patrec.2005.10.010

Feng, X. (2019). Global maps of seasonality indices, HydroShare. https://www.hydroshare.org/resource/ff287c90c9e947a78e351c8d07d9d3f3

Feng, X., Porporato, A., & Rodriguez-Iturbe, I. (2013). Changes in rainfall seasonality in the tropics. *Nature Climate Change*, *3*(9), 811–815. https://doi.org/10.1038/nclimate1907

Feng, X., Porporato, A., Rodriguez-Iturbe, I., & Rodríguez-Iturbe, I. (2015). Stochastic soil water balance under seasonal climates. *Proceedings of the Royal Society A: Mathematical, Physical and Engineering Sciences*, *471*(2174). https://doi.org/10.1098/rspa.2014.0623

Feng, X., Vico, G., & Porporato, A. (2012). On the effects of seasonality on soil water balance and plant growth. *Water Resources Research*, *48*, W05543. https://doi.org/10.1029/2011WR011263

Gentine, P., D'Odorico, P., Lintner, B. R., Sivandran, G., & Salvucci, G. (2012). Interdependence of climate, soil, and vegetation as constrained by the Budyko curve. *Geophysical Research Letters*, *39*, L19404. https://doi.org/10.1029/2012GL053492

Giorgi, F. (2006). Climate change hot-spots. *Geophysical Research Letters*, *33*(8), L08707. https://doi.org/10.1029/2006GL025734

Hahm, W. J., Dralle, D. N., Rempe, D. M., Bryk, A. B., Thompson, S. E., Dawson, T. E., & Dietrich, W. E. (2019). Low subsurface water storage capacity relative to annual rainfall decouples Mediterranean plant productivity and water use from rainfall variability. *Geophysical Research Letters*, *46*, 6544–6553. https://doi.org/10.1029/2019GL083294

Hanley, J. A., & Mcneil, B. J. (1982). Meaning and use of the area under a receiver operating curve. *Radiology*, *143*(1), 29–36. https://doi.org/10.1148/radiology.143.1.7063747

Harris, I., Jones, P. D., Osborn, T. J., & Lister, D. H. (2014). Updated high-resolution grids of monthly climatic observations—The CRU TS3.10 Dataset. *International Journal of Climatology*, *34*(3), 623–642. https://doi.org/10.1002/joc.3711

Iglesias, A., Garrote, L., Flores, F., & Moneo, M. (2007). Challenges to manage the risk of water scarcity and climate change in the Mediterranean. *Water Resources Management*, *21*(5), 775–788. https://doi.org/10.1007/s11269-006-9111-6

IPCC (2014). Summary for policymakers. Climate Change 2014: Synthesis Report. Contribution of Working Groups I, II and III to the Fifth Assessment Report of the Intergovernmental Panel on Climate Change. https://doi.org/10.1017/CBO9781107415324

Jeton, A. E., Dettinger, M. D., & Smith, J. L. (1996). Potential effects of climate change on streamflow, eastern and western slopes of the Sierra Nevada. California and Nevada. U.S. Gelogical Survey. Sacramento, California.

Klausmeyer, K. R., & Shaw, M. R. (2009). Climate change, habitat loss, protected areas and the climate adaptation potential of species in Mediterranean ecosystems worldwide. *PLoS ONE*, *4*(7), e6392. https://doi.org/10.1371/journal.pone.0006392

Knoben, W. J. M., Woods, R. A., & Freer, J. E. (2018). A quantitative hydrological climate classification evaluated with independent streamflow data. *Water Resources Research*, *54*, 5088–5109. https://doi.org/10.1029/2018WR022913

Kottek, M., Grieser, J., Beck, C., Rudolf, B., & Rubel, F. (2006). World map of the Köppen-Geiger climate classification updated. *Meteorologische Zeitschrift*, *15*(3), 259–263. https://doi.org/10.1127/0941-2948/2006/0130

Kraft, N. J. B., Adler, P. B., Godoy, O., James, E. C., Fuller, S., & Levine, J. M. (2014). Community assembly, coexistence and the environmental fi ltering metaphor. *Functional ecology*, *29*(5), 592–599. https://doi.org/10.1111/1365-2435.12345

Kullback, S., & Leibler, R. A. (1951). On information and sufficiency. *The Annals of Mathematical Statistics*, *22*(1), 79–86.

Maestre, F. T., Delgado-Baquerizo, M., Jeffries, T. C., Eldridge, D. J., Ochoa, V., Gozalo, B., et al. (2015). Increasing aridity reduces soil microbial diversity and abundance in global drylands. *Proceedings of the National Academy of Sciences of the United States of America*, *112*(51), 15684–15689. https://doi.org/10.1073/pnas.1516684112

Matusick, G., Ruthrof, K. X., Brouwers, N. C., Dell, B., & Hardy, G. S. J. (2013). Sudden forest canopy collapse corresponding with extreme drought and heat in a Mediterranean-type eucalypt forest in southwestern Australia. *European Journal of Forest Research*, *132*(3), 497–510. https://doi.org/10.1007/s10342-013-0690-5

Médail, F., & Quezél, P. (1999). Biodiversity hotspots in the Mediterranean Basin: Setting global conservation priorities. *Conservation Biology*, *13*(6), 1510–1513.

Metzger, M. J., Bunce, R. G. H., Jongman, R. H. G., Sayre, R., Trabucco, A., & Zomer, R. (2013). A high-resolution bioclimate map of the world: A unifying framework for global biodiversity research and monitoring. *Global Ecology and Biogeography*, *22*, 630–638. https://doi.org/10.1111/geb.12022

Milly, P. C. D. C. D. (1994). Climate, interseasonal storage of soil water, and the annual water balance. *Advances in Water Resources*, *17*(1–2), 19–24. https://doi.org/10.1016/0309-1708(94)90020-5

Musselman, K. N., Clark, M. P., Liu, C., Ikeda, K., & Rasmussen, R. (2017). Slower snowmelt in a warmer world. *Nature Climate Change*, *7*(3), 214–219. https://doi.org/10.1038/nclimate3225

Oliver, J. E. (1991). The history, status and future of climate classification. *Physical Geography*, *12*(3), 231–251.

Paltineanu, C., Tanasescu, N., Chitu, E., & Mihailescu, I. F. (2007). Relationships between the De Martonne aridity index and water requirements of some representative crops: A case study from Romania. *International Agrophysics*, *21*(1), 81–93.

Pangle, L. A., Gregg, J. W., & McDonnell, J. J. (2014). Rainfall seasonality and an ecohydrological feedback offset the potential impact of cimate warming on evapotranspiration and groundwater recharge. *Water Resources Research*, *50*, 1308–1321. https://doi.org/10.1002/2012WR013253

Peel, M. C., Finlayson, B. L., & McMahon, T. A. (2007). Updated world map of the Köppen-Geiger climate classification. *Hydrology and Earth System Sciences Discussions*, *4*(2), 439–473.

Petrone, K. C., Hughes, J. D., Van Niel, T. G., & Silberstein, R. P. (2010). Streamflow decline in southwestern Australia, 1950-2008. *Geophysical Research Letters*, *37*, L11401. https://doi.org/10.1029/2010GL043102

Potter, N. J., Zhang, L., Milly, P. C. D., Mcmahon, T. A., & Jakeman, A. J. (2005). Effects of rainfall seasonality and soil moisture capacity on mean annual water balance for Australian catchments. *Water Resources Research*, *41*, W06007. https://doi.org/10.1029/2004WR003697

Razavi, T., & Coulibaly, P. (2013). Streamflow prediction in ungauged basins: Review of regionalization methods. *Journal of Hydrologic Engineering*, *18*(8), 958–975. https://doi.org/10.13243/j.cnki.slxb.20160069

Ryu, Y., Baldocchi, D. D., Ma, S., & Hehn, T. (2008). Interannual variability of evapotranspiration and energy exchange over an annual grassland in California. *Journal of Geophysical Research*, *113*, D09104. https://doi.org/10.1029/2007JD009263

Seager, R., Liu, H., Henderson, N., Simpson, I., Kelley, C., Shaw, T., et al. (2014). Causes of increasing aridification of the Mediterranean region in response to rising greenhouse gases. *Journal of Climate*, *27*(12), 4655–4676. https://doi.org/10.1175/JCLI-D-13-00446.1

Staten, P. W., Lu, J., Grise, K. M., Davis, S. M., & Birner, T. (2018). Re-examining tropical expansion. *Nature Climate Change*, *8*(9), 768–775. https://doi.org/10.1038/s41558-018-0246-2

Stöckle, C. O., Higgins, S., Nelson, R., Abatzoglou, J., Huggins, D., Pan, W., et al. (2018). Evaluating opportunities for an increased role of winter crops as adaptation to climate change in dryland cropping systems of the U.S. Inland Pacific Northwest. *Climatic Change*, *146*(1–2), 247–261. https://doi.org/10.1007/s10584-017-1950-z

Tague, C., & Peng, H. (2013). The sensitivity of forest water use to the timing of precipitation and snowmelt recharge in the California Sierra: Implications for a warming climate. *Journal of Geophysical Research: Biogeosciences*, *118*, 875–887. https://doi.org/10.1002/jgrg.20073

Thomas, N., & Nigam, S. (2018). Twentieth-century climate change over Africa: Seasonal hydroclimate trends and sahara desert expansion. *Journal of Climate*, *31*(9), 3349–3370. https://doi.org/10.1175/JCLI-D-17-0187.1

Timbal, B., Arblaster, J. M., & Power, S. (2006). Attribution of the late-twentieth-century rainfall decline in southwest Australia. *Journal of Climate*, *19*(10), 2046–2062. https://doi.org/10.1175/JCLI3817.1

Trancoso, R., Phinn, S., McVicar, T. R., Larsen, J. R., & McAlpine, C. A. (2017). Regional variation in streamflow drivers across a continental climatic gradient. *Ecohydrology*, *10*(3). https://doi.org/10.1002/eco.1816

Underwood, E. C., Viers, J. H., Klausmeyer, K. R., Cox, R. L., & Shaw, M. R. (2009). Threats and biodiversity in the Mediterranean biome. *Diversity and Distributions*, *15*(2), 188–197. https://doi.org/10.1111/j.1472-4642.2008.00518.x

Varenius, B. (1650). *Geographia Generalis*. Amsterdam: Elzevir.

Vico, G., & Porporato, A. (2015). Ecohydrology of agroecosystems: Quantitative approaches towards sustainable irrigation. *Bulletin of Mathematical Biology*, *77*(2), 298–318. https://doi.org/10.1007/s11538-014-9988-9

Vico, G., Thompson, S. E., Manzoni, S., Molini, A., Albertson, J. D., Almeida-Cortez, J. S., et al. (2014). Climatic, ecophysiological and phenological controls on plant ecohydrological strategies in seasonally dry ecosystems. *Ecohydrology*, *8*(4), 660–681. https://doi.org/10.1002/eco.1533

Viola, F., Daly, E., Vico, G., Cannarozzo, M., & Porporato, A. (2008). Transient soil-moisture dynamics and climate change in Mediterranean ecosystems. *Water Resources Research*, *44*, W11412. https://doi.org/10.1029/2007WR006371

von Humboldt, A. (1820). On the isothermal lines, and the distribution of heat on the globe. Archibald Constable.

Walsh, R. P. D., & Lawler, D. M. (1981). Rainfall seasonality: Description, spatial patterns and change through time. *Weather*, *36*(7), 201–208. https://doi.org/10.1002/j.1477-8696.1981.tb05400.x

Wang, C., Wang, X., Liu, D., Wu, H., Lü, X., Fang, Y., et al. (2014). Aridity threshold in controlling ecosystem nitrogen cycling in arid and semi-Arid grasslands. *Nature Communications*, *5*(1), 4799. https://doi.org/10.1038/ncomms5799

Wang, D., & Hejazi, M. (2011). Quantifying the relative contribution of the climate and direct human impacts on mean annual streamflow in the contiguous United States. *Water Resources Research*, *47*, W00J12. https://doi.org/10.1029/2010WR010283

Winchell, T. S., Barnard, D. M., Monson, R. K., Burns, S. P., & Molotch, N. P. (2016). Earlier snowmelt reduces atmospheric carbon dioxide uptake in midlatitide subalpine forests. *Geophysical Research Letters*, *43*, 8160–8168. https://doi.org/10.1002/2016GL069769.Received

Wolf, S., Keenan, T. F., Fisher, J. B., Baldocchi, D. D., Desai, A. R., Richardson, A. D., et al. (2016). Warm spring reduced carbon cycle impact of the 2012 US summer drought. *Proceedings of the National Academy of Sciences of the United States of America*, *113*(21), 5880–5885. https://doi.org/10.1073/pnas.1519620113

Woods, R. A. (2009). Analytical model of seasonal climate impacts on snow hydrology: Continuous snowpacks. *Advances in Water Resources*, *32*(10), 1465–1481. https://doi.org/10.1016/j.advwatres.2009.06.011

Zhang, H., & Oweis, T. (1999). Water-yield relations and optimal irrigation scheduling of wheat in the Mediterranean region. *Agricultural Water Management*, *38*(3), 195–211. https://doi.org/10.1016/S0378-3774(98)00069-9